

# Particle analysis by laser mass spectrometry (PALMS) studies of ice nuclei and other low number density particles

Daniel J. Cziczo<sup>a,\*</sup>, David S. Thomson<sup>b,c</sup>, Thomas L. Thompson<sup>b</sup>,  
Paul J. DeMott<sup>d</sup>, Daniel M. Murphy<sup>b</sup>

<sup>a</sup> *Institute for Atmosphere and Climate Science, ETH Zurich 8092, Switzerland*

<sup>b</sup> *Chemical Sciences Division, Earth System Research Lab, National Oceanic and Atmospheric Administration, Boulder, CO 80305, USA*

<sup>c</sup> *Cooperative Institute for Research in Environmental Sciences, University of Colorado, Boulder, CO 80309, USA*

<sup>d</sup> *Department of Atmospheric Science, Colorado State University, Fort Collins, CO 80523, USA*

Received 12 March 2006; received in revised form 12 May 2006; accepted 17 May 2006

Available online 19 June 2006

## Abstract

It has been shown that particles which effectively initiate freezing, known as ice nuclei (IN), are normally found at concentrations less than  $10^{1-1}$  in the background atmosphere. The low number density of these particles has presented significant analytical challenges, and determination of the size and composition, and thus the origin, of these particles has historically relied upon electron microscopy (EM). Single particle mass spectrometers can provide better time resolution and reduced sampling artifacts. The modifications to the particle analysis by laser mass spectrometry (PALMS) instrument, a laser desorption/ionization mass spectrometer, required to efficiently size and analyze particles with very low number density, are described here. A comparison to traditional EM studies is made and future applications of this method to solve other contemporary atmospheric problems are also discussed.

© 2006 Elsevier B.V. All rights reserved.

**Keywords:** Aerosol mass spectrometry; Laser desorption/ionization; Ice nuclei

## 1. Introduction

The first attempts several decades ago to desorb and ionize aerosol components and analyze them using mass spectrometry were hampered by inadequate technology [1]. With the advent of adequate vacuum systems and lasers, several groups were able to produce high signal-to-noise mass spectra in laboratory experiments and at field sites [2–5]. Since that time single particle mass spectrometers have improved significantly. These instruments have provided a previously unavailable means of determining the chemical composition of atmospheric aerosol particles which has changed many of our previously held views regarding atmospheric particle formation, transformation and removal [6–8]. The vast majority of data taken by aerosol mass spectrometers has been at ground level. While the number density of particles between 200 nm and 2  $\mu\text{m}$  diameter, a fairly average window of

accessible particle sizes for contemporary instruments, is highly variable, it is normally no less than  $100\text{ cm}^{-3}$  in remote locations [9]. Even in cases where single particle instruments have been flown into the stratosphere number densities at the highest attained altitudes ( $\sim 20\text{ km}$ ) in this size window normally exceed  $0.5\text{ cm}^{-3}$  [10].

There are atmospherically relevant issues, which are dependent on particles with much lower number densities, however. For example, cirrus ice clouds are known to exert a large radiative forcing on the Earth's climate system due to the combination of their high altitude and large global coverage [11]. Experimental studies of the aerosols which readily nucleate ice, and thus likely form the basis for ice cloud formation, have shown that such particles, termed ice nuclei, have a typical abundance of only between 1 and  $10^{1-1}$  [12]. Past studies of IN size have relied on electron microscopy because the technique is sensitive at the single particle level. Studies in the free troposphere over the central United State, for example, found a mode size for efficient ice forming aerosols between 100 nm and 1  $\mu\text{m}$  geometric diameter with a peak at  $\sim 200\text{ nm}$  [13]. With the addition

\* Corresponding author. Tel.: +41 446332745; fax: +41 446331058.  
E-mail address: [daniel.cziczo@env.ethz.ch](mailto:daniel.cziczo@env.ethz.ch) (D.J. Cziczo).

of energy dispersive X-ray analysis, chemical composition of IN was made possible and it was found that most IN are composed of refractory elements, such as mineral dust or metal oxides [13–15]. EM is, however, an off-line technique and significant care must be taken to prevent artifacts during sample handling and preparation [16]. The labor intensity required has restricted past studies to 100's of particles. Analysis takes place in vacuo and volatile materials are not discernable. IN components are also indistinguishable if they have the same composition as the sample substrate.

Laser desorption/ionization mass spectrometry is known to have several important limitations [17]. For example, ionization efficiencies for common aerosol components can be widely disparate, mass spectral characteristics can be highly dependent on particle matrix and the surface of large and/or highly refractory particles can be over-sampled with respect to the bulk [17]. Despite these limitations, the on-line nature, high signal-to-noise and sensitivity to volatile and refractory components renders laser desorption/ionization mass spectrometry superior to traditional electron microscope analyses of ice nuclei.

Several groups now employ techniques to determine the size and chemical composition of atmospheric aerosols using mass spectrometry. Other instruments, many of these described in detail within this special issue, have comparable, and in some cases superior, capabilities. The purpose of this publication is to describe the modification made to the particle analysis by laser mass spectrometry instruments to facilitate our investigation of

low number density species, such as ice nuclei, to document the current status of the instruments and to quantify the performance of these modifications.

## 2. Experimental

The particle analysis by laser mass spectrometry instrument has been described in detail previously [18,19]. There are two PALMS instruments. The 'ground instrument' was originally designed and built in the early 1990's. It serves dual functions as a ground based single particle instrument used in laboratory [20,21] and field [22,23] studies and as a prototype and testbed for the second 'flight instrument'. The PALMS ground and flight versions have essentially identical components and performance with the exception of the aerodynamic inlets and computers described in the next sections. The other major difference between the two instruments is that the flight instrument is more compact so as to fit within the confined space of the nose of a NASA WB-57F high altitude research aircraft and later a wing pod on the NOAA P-3 [19,24]. Additional differences, related to the power, heating and vibration isolation requirements of a flight instrument, also exist but are not relevant to the discussion here. Since the previous PALMS instrument technical publications the ground and flight instruments have undergone changes. In the case of the ground instrument, these modifications were undertaken in order to perform studies of the chemical composition of ice nuclei at the Desert Research

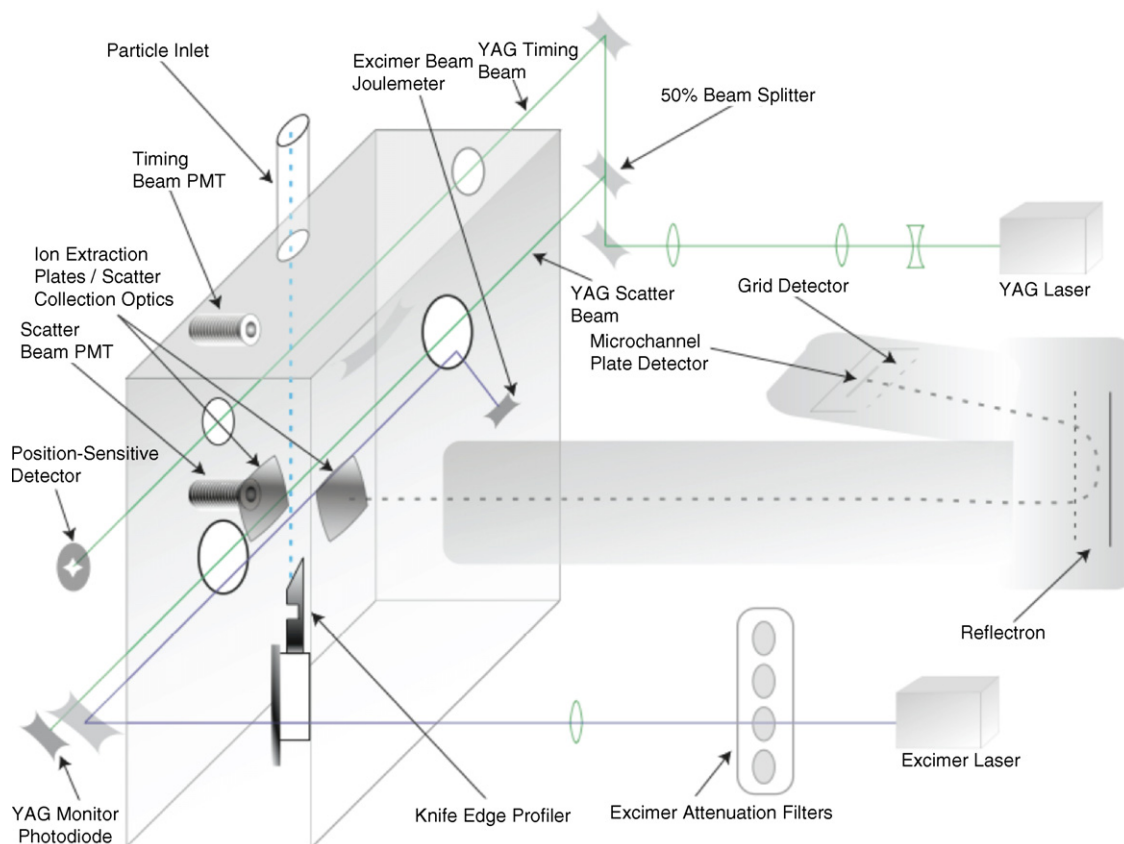


Fig. 1. Schematic diagram of the PALMS instrument.

Institute's Storm Peak Laboratory [25] during the Ice Nuclei SPECTrometry (INSPECT) missions in 2001 and 2004. Similar changes were made to the PALMS flight instrument for in situ studies of anvil cirrus clouds from aboard the NASA WB-57F during the 2002 Cirrus Regional Study of Tropical Anvils and Cirrus Layers-Florida Area Cirrus Experiment (CRYSTAL-FACE) [26]. Various other modification were made to increase acquisition rate and overall data quality during these and other missions. A current schematic of the PALMS instruments is shown in Fig. 1.

A fundamental prerequisite of IN studies is the efficient separation of sparse ice crystals ( $10^1$ ) from higher number density unactivated, or 'interstitial', aerosol (typically  $>10^6$ ). Pumped and traditional counterflow virtual impaction (CVI) was utilized [27]. While ice crystals form on sub-micrometer aerosols they rapidly acquire mass via uptake of water vapor and reach several to several 10's of micrometers diameter. The inertial difference forms the basis of the CVI technique. A flow of dry, particle free, gas – the counterflow – is directed against the particle flow – containing both ice crystals and unactivated aerosol – such that particles with insufficient inertia are stopped and pumped away. The rate of counterflow is thus set so as to create a cutpoint that allows passage of ice crystals for analysis but rejects all unactivated aerosol.

### 2.1. Inlet and vacuum

The major difference between the PALMS ground and flight versions is the inlet system used to draw particles into the instrument and focus them for optimal detection and analysis. The flight instrument uses an isobaric ( $\sim 40$  mb) aerodynamic inlet based on the design of Schreiner [28]. This inlet is superior to a simple capillary used before 2002 in that it exhibits relatively constant transmission with respect to particle size over the detectable range of  $\sim 150$  nm to  $2.0$   $\mu\text{m}$ . Transmission is also significantly higher, by several orders of magnitude, for the smallest particles when compared with the old capillary inlet. Furthermore, the pressure control of this inlet means that the performance is not dependent on altitude, which can range from a few hundred meters above mean sea level (m msl) on the NOAA P-3 up to 19 km on the NASA WB-57F. The transmission properties of the flight inlet have been described previously and are not repeated here [26].

The main concern in the case of the ground instrument was not transmission independence over a large altitude range. Instead, the ratio of particles transmitted to the detection and analysis region of the instrument versus the number of particles present before the inlet was the quantity to be optimized. The basis for this design is the work of Liu et al. [29] and Jayne et al. [30] and is used by several other contemporary mass spectrometers [31,32]. The PALMS inlet is operated at about a factor of five times higher pressure, set by a  $200$   $\mu\text{m}$  diameter critical orifice, than this nominally  $2$  mb aerodynamic lens. The length of the lens is  $40$  cm with a total of five orifices spaced at  $5$  cm intervals. The orifice size is stepped down incrementally with inner diameters of  $0.50$ ,  $0.45$ ,  $0.40$ ,  $0.375$  and  $0.30$  cm. It should be noted that the PALMS flight and ground inlets are constructed with

the same interface to the detection and analysis region. While the aerodynamic lenses have been designed to optimize particle collection in the unique regimes encountered by the two instruments, they are completely interchangeable with each other and with past inlets for testing and calibration purposes.

The transmission efficiency of the ground inlet was determined by preparing three different test aerosols using a BGI Inc. 1-Jet Collision nebulizer. Two of the three test aerosols, polystyrene latex (PSL) spheres and Arizona test dust (ATD), are insoluble and therefore were produced from a suspension in distilled, deionized water. The third test aerosol, ammonium nitrate, was nebulized directly from a  $20$  wt% solution in distilled, deionized water. Aerosol was subsequently passed through a diffusion dryer to remove condensed phase water at  $50\%$  relative humidity and size selected using a NOAA-designed differential mobility analyzer (DMA). The  $500$  sccm output of the DMA was balanced with dry, particle-free air and split into two flows:  $300$  sccm to the PALMS ground instrument and  $300$  sccm to a TSI model 3020 CPC. The transmission efficiency was defined as the number of particles which produced a mass spectrum in the PALMS instrument per inlet flow volume versus the number density counted by the CPC (i.e., the number of particles present before the aerodynamic inlet). This data is shown in Fig. 2 for the three particle types at two different ambient pressures. These pressures correspond to the two discrete altitudes of recent PALMS sites: the NOAA Earth System Research Lab in Boulder, Colorado ( $1600$  m msl), and the Storm Peak Laboratory in Steamboat Springs, Colorado ( $3210$  m msl).

Particle transmission efficiency in Fig. 2 is plotted against vacuum aerodynamic diameter. This is the relevant quantity for most contemporary aerosol mass spectrometers that use low pressure aerodynamic focusing lenses [33]:

$$d_{va} = d_p \left[ \frac{\rho_p}{\rho_0} \right] \quad (1)$$

where  $d_{va}$  is the vacuum aerodynamic and  $d_p$  is the particle physical diameter. For spherical particles, such as PSL and ammonium nitrate, the physical diameter is equal to the mobility diameter, which is the quantity selected by a DMA. The particle density is given as  $\rho_p$  versus a reference density  $\rho_0$  of  $1$  g  $\text{cm}^{-3}$ . For simplicity it is assumed that this relationship remains valid for the ATD samples, although these particles are known to be somewhat non-spherical [34]. The motivation to investigate ATD was to better understand the transmission and detection of non-spherical particles with a composition mimicking that previously found for IN [13–15].

The PALMS instrument produces a mass spectrum from  $\sim 95\%$  of detected particles [25]. Losses are due to a combination of: (a) particles with a trajectory that passes through the detection laser beam but which do not pass through the desorption/ionization beam, (b) very small and thus high velocity, particles which travel past the desorption/ionization laser before it is triggered or, conversely, very large particles with low velocity which do not travel into the desorption/ionization beam before it is triggered and (c) very pure particles of difficult-to-ionize substances. These topics are discussed in detail in the

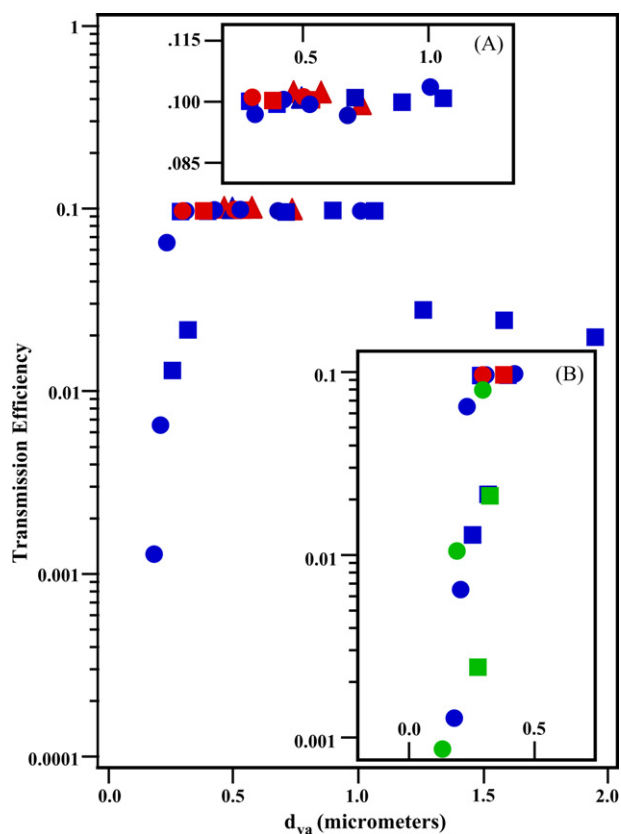


Fig. 2. Transmission efficiency of particles as a function of vacuum aerodynamic diameter for the PALMS instrument. The value represents the ratio of particles which produced a mass spectrum to the total number density before the inlet (see text for details). Particle types are differentiated by shapes: PSL spheres ( $\rho = 1.05 \text{ g/cm}^3$ , circles), ammonium nitrate ( $\rho = 1.7 \text{ g/cm}^3$ , squares) and Arizona test dust ( $\rho \sim 2.5 \text{ g/cm}^3$ , triangles). Blue shapes indicate data acquired at 625 Torr (Boulder, CO) and red shapes data acquired at 520 Torr (Storm Peak Laboratory, CO). *Inset*: Panel A expands for clarity, with a linear scale, the relatively flat transmission region. *Inset*: Panel B expands the falloff region at small diameter using green shapes for additional data acquired at 715 Torr (Zurich, Switzerland).

next section but it is noted here since the transmission efficiency contains these inherent 5% missed trajectory and mismatched velocity effects.

From approximately 300 nm to 1  $\mu\text{m}$  diameter, the transmission efficiency is essentially constant at one particle analyzed per 10 incident aerosols. This region is expanded on a linear scale in panel A of Fig. 2 for clarity. The performance does not exhibit a dependence on inlet pressure from 625 to 520 mb (i.e., 1600–3210 m msl altitude). The reduction in transmission efficiency above  $\sim 1 \mu\text{m}$  diameter is due to the velocity effect as well as reduced performance observed for large particles due to aerodynamic overcorrection in similar aerodynamic inlets [35]. Additional tests were performed in Zurich, Switzerland (500 m msl) to investigate the lower detection limit. These data are shown in panel B. For PSL spheres the transmission efficiency drops by more than two orders of magnitude from 300 to 150 nm. A 125 nm diameter PSL spheres were not detected. The transmission efficiency is lower, at a given aerodynamic diameter, for ammonium nitrate particles. This is likely due to their smaller physical size at a given aerodynamic diameter due

to a larger density. 200 nm ammonium nitrate particles were not detected.

Recent work by Huffman et al. [36] on a similar inlet used in the aerodyne aerosol mass spectrometer (AMS) assumes that the output of an aerodynamic lens is a point source. This is a good approximation for a system with a long travel distance and large target, such as the AMS, but it is not an adequate description for instruments such as PALMS. Specifically, the output of an aerodynamic lens has a finite diameter of about 100  $\mu\text{m}$  [37], which is essentially identical to the width of the PALMS detection laser beam (see next section). Thus, any divergence will lead to less than 100% particle transmission to the detection region. Huffman et al. [36] describe the standard deviation of the particle beam for several aerodynamic lenses as a function of target distance and inlet pressure. While this is the relevant quantity for the AMS, single particle mass spectrometry geometry is typically somewhat different. For PALMS, it can be approximated by detection and analysis of particles within a 100  $\mu\text{m}$  wide strip 55 mm from the end of the inlet (i.e., the width and location of the detection laser relative to the lens output). Given a particle beam with initial diameter 100  $\mu\text{m}$  and a three sigma divergence of approximately  $0.5^\circ$  this results in 10% of particles passing through the detection beam. Huffman et al. [36] also shows that particle shape leads to larger divergences, typically by a factor of 2–5 in the case of highly non-spherical particles, such as soot. The lack of a clear reduction in transmission for mineral dust, although it is not as highly non-spherical as soot, is also tied to the PALMS geometry. The larger non-spherical divergence effect is of second order to the superposition of the particle beam on the detection laser. A three sigma divergence a factor of two higher would, for example, result in only  $\sim 10\%$  differences in the transmission efficiency.

## 2.2. Lasers and optics

Much of the optical design of the PALMS instruments remains similar to that described previously [19]. As shown in Fig. 1, a 532 nm continuous wave (CW) neodymium:yttrium–aluminum–garnet (YAG) laser detection beam is counter-propagating with respect to the 193 nm pulsed excimer ionization laser beam. The primary change to the optical design is the addition of the second ‘timing’ YAG beam. As can be seen in Fig. 1, the primary YAG beam steering mirror has been replaced with a 50% beam splitter. Whereas a single 80 mW CW YAG beam was previously used for particle detection, a 100 mW YAG laser is now used (Coherent/Adlas Model DPY 315M), resulting in a 50 mW main particle detection beam being reflected from the beam splitter. No appreciable loss in performance accompanied this reduction in laser power since the minimum detectable particle size was previously limited by YAG laser noise, not by YAG laser power or amplifier noise.

The timing YAG beam was created by adding an additional optical section to the vacuum system above the source region but below the focusing inlet. This second beam is parallel to the primary particle detection beam and is separated from it by 33.6 mm. Since the same focusing optics are used by both beams

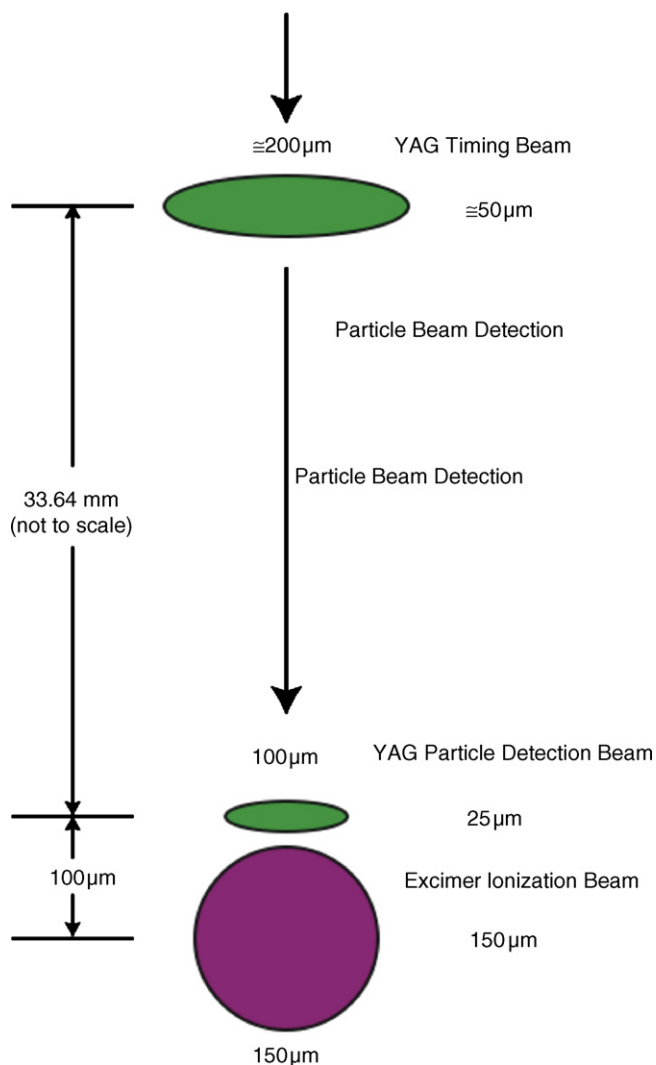


Fig. 3. PALMS laser beam focus geometry. The diagram shows the laser beam dimensions at the intersection of the laser beams and the particle beam as viewed along the direction of the laser beam propagation. The laser beam sizes are specified as the full-width-half-max of the Gaussian profile. The excimer beam is significantly non-Gaussian, but is still specified by the FWHM of the Gaussian fit to its profile.

before the beam splitter, the focus of the upper beam is adjusted for the additional 33 mm of path length by using a convex mirror with a 1.5 m radius of curvature for the turning mirror. This results in the focus of the timing beam being near the intersection of the timing beam with the particle beam. Whereas the collection optics for the particle detection beam are integrated with the ion extraction plates [19], the timing beam collection optics have no such dual function and could therefore be better optimized for light collection. Thus, it is not necessary for the timing beam focus to be held to the same requirements as the particle detection beam focus. The geometry of all three laser beam foci is shown in Fig. 3.

Triggering of the desorption laser remains exclusively due to particles crossing the detection laser beam. As such, an aerosol need not pass through the timing beam although typically >90% of the particles which yield mass spectra also yield signals from the timing YAG beam.

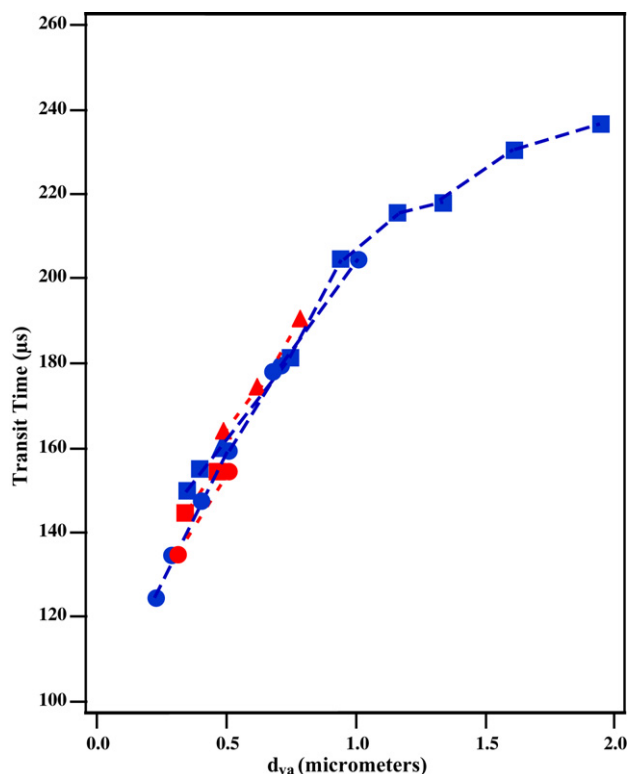


Fig. 4. Transmission time between the PALMS detection laser beams as a function of vacuum aerodynamic diameter. Particle types are differentiated by shapes: PSL spheres ( $\rho = 1.05 \text{ g/cm}^3$ , circles), ammonium nitrate ( $\rho = 1.7 \text{ g/cm}^3$ , squares) and Arizona test dust ( $\rho \sim 2.5 \text{ g/cm}^3$ , triangles). Blue points, connected with a dashed line, indicate data acquired at 625 Torr (Boulder, CO) and red points, connected with a dotted line, data acquired at 520 Torr (Storm Peak Laboratory, CO).

As seen in Fig. 3, the YAG foci are elliptical, which is accomplished by the use of cylindrical lenses. By concentrating the laser beam along the axis of the particle beam two advantages are obtained for the particle detection beam. First, reducing the size of the beam in this direction increases the power density of the beam, giving larger signals. Second, reducing this dimension reduces the difference in trigger time between small and large particles. Small particles near the detection limit of the system will only generate a trigger when they are at the central peak intensity of the beam, whereas large particles scatter enough light to generate a trigger when they are just entering the edge of the beam. If the beam had significant extent in this dimension, this could result in measurable trigger timing differences. Since large particles have a lower velocity than small particles, this timing difference would compound the velocity dispersion effect and make it even more difficult to hit large and small particles with the same excimer laser beam focus. The current design renders the addition of a trigger delay for large particles unnecessary. The beam ellipticity has no significant effect on the timing laser beam. Particle velocity is determined by the timing between the maxima of the two scattered light signals, and is therefore insensitive to the points within the beams that the signal first exceeds a threshold. This time is plotted as a function of aerodynamic diameter in Fig. 4, thus illustrating the ability to derive particle size from the time difference between

light scattering events from the timing and detection laser beams. This technique has been employed to determine aerosol size in several instrument types [16] and incorporated into single particle laser desorption/ionization mass spectrometers [31,32]. Murphy et al. [38] have shown that when refractive index can be assumed constant the absolute scattering from the detection beam provides an optical particle size. Determination of the aerodynamic size from the transit time between the detection and timing can be coupled with particle density inferred from the mass spectral composition to return a geometric diameter that agrees well with the light scattered from only the detection beam.

All three laser beams have motorized steering mirrors and positioning feedback. The two-edged profiler used to measure the positions and widths of the excimer and particle detection beams has been described previously [19]. The timing beam incorporates a different feedback mechanism. A position sensitive detector (Hamamatsu S2044) is placed outside the vacuum system but within a few centimeters of the beam focus. At this location, the laser beam has not diverged significantly and is therefore well resolved on the 4.7 mm × 4.7 mm detector surface. In addition, this two-dimensional position sensitive detector responds only to the centroid of the laser beam, not the beam size. By measuring the resistance between the four leads of the pin-cushion shaped active area of this detector, the two-dimensional position can be calculated. This detector is not calibrated absolutely to the source region, but rather the best position is found empirically, and then the motorized mirror is used to maintain that position during operation.

The detector for the timing beam signal is a Hamamatsu model 5600 photomultiplier tube, which is the same used for the particle detection beam. Due to space constraints, the turning mirror used is a miniature version of the New Focus Picomotor mounts previously described [19]. The New Focus model 8883 Pint-Size mount is only 3.175 cm across compared to 6.35 cm for the model 8809 Picomotor mount, and uses a smaller version of the Picomotor actuators.

### 2.3. Electronic components

The electronics of the PALMS instrument are nearly functionally equivalent to those described previously. Several items have been upgraded in the past few years for improved performance and reliability, however. The computer for the PALMS flight instrument has been changed to a Tyan S1854 Trinity 400 motherboard with a 533MHz PIII processor. This motherboard and processor have been tested for operation at the reduced pressures experienced during flight. Another improvement that has been made to this system is the replacement of a pressure-sealed mechanical hard disk with an 8 GB solid state hard disk (Memtech 32550A) in a removable drive bay. Although this solid state hard disk has significantly faster read and write times than those of a few years ago, it remains slower than a mechanical disk and limits the data acquisition rate to about 10 events per second. In addition to being able to run at reduced pressures, the solid state hard disk can operate in significantly higher vibrational environments than a mechanical hard disk.

The computer of the PALMS ground instrument has also been upgraded. Since it operates in higher pressure environments, a more modern computer has been integrated into this instrument. It currently uses a SuperMicro P4SCA motherboard with a 1.5 GHz P4 processor. Using a mechanical hard disk for ground-based work, the instrument can acquire data at 20 events per second.

The digitizers for the mass spectrometer signal and scattered light signal have been upgraded to 500 MS/s, 8 bit Acqiris DP210 digitizers. Our tests have shown this model to have at least 7.5 effective bits of resolution. The oversampling resulting from the increase in speed from our previous 200 MS/s digitizers also improves the signals. In addition, the thermal design of these PCI cards makes it possible to run them at the reduced pressure of one-third atmosphere experienced by the flight instrument or at 3210 m msl altitudes experienced by the ground instrument without additional cooling.

The PALMS instruments have three high voltage power supplies. Two of them are of similar design, using high-voltage dc-dc converters (Brandenburg 4479) to provide the PMT and micro-channel plate (MCP) voltages. The third high voltage supply provides 10 different values for the various mass spectrometer bias voltages. This high voltage supply was redesigned to provide better reliability and increased flexibility in tuning the mass spectrometer voltages. The new high voltage power supply (HVPS) is controlled by a microprocessor that communicates to the PALMS instrument via an RS232 serial port. The microprocessor specifies the set-points for the 10 high-voltage outputs and reports the measured voltages of these outputs back to the PALMS instrument. The accuracy of the high-voltage output is approximately 0.3%. The scaled voltage is also monitored by A/D converters controlled by the microprocessor, which then reports these readings back to the main PALMS computer.

### 2.4. Software

The software for the PALMS instrument has been improved since the last published description [19,39], but the over-all structure remains the same. The program is now written in LabVIEW version 7.1 and runs under Windows 2000. The last several years have seen a significant movement within the LabVIEW programming community to incorporate Object Oriented Programming concepts into LabVIEW, which itself is not inherently an object oriented language. The PALMS program is most similar in concept to the LabVIEW Component Oriented Design (LCOD) described by Conway and Watts [40], though the PALMS architecture was developed in parallel to LCOD. The primary change to the PALMS program in recent years is making each of the 'drivers' (logical software components that each handle a specific hardware device, virtual device or task) a more complete and coherent component or object. Previously, the main PALMS program was responsible for initializing each driver, and for doing so in the proper order to support the hierarchical nature of the drivers. Now, the configuration information for each driver is accessed by the driver itself. Furthermore, each driver can read the configuration information and initialize itself automatically if a call is made to that driver before it has been

explicitly initialized. Since the drivers are hierarchical, a call to one driver can require access to many other lower-level drivers. This results in a more robust implementation, easier debugging and a simpler user interface.

### 3. Results and discussion

The PALMS ground instrument has been deployed during the two INSPECT field campaigns to determine the composition of ice forming aerosols. These studies took place at the remote mountain-top Storm Peak Laboratory. For this work the Colorado State University Continuous Flow Diffusion Chamber (CFDC) was used to mimic the temperature and humidity conditions that initiate ice formation within high altitude cirrus clouds [41]. The mass spectra of  $\sim 2500$  aerosols which nucleated ice were acquired. The following discussion is restricted to the several hundred aerosols which formed ice by heterogeneous nucleation, that is due to the specific action of a contained insoluble particle surface, and with a typical abundance of  $1\text{--}10\text{1}^{-1}$ . The addition of the PALMS timing beam took place in 2003 and aerodynamic diameters are available for particles analyzed during the second INSPECT mission. Ice crystals formed within the CFDC were separated from those particles which did not form ice using a pumped counterflow virtual impactor [25,27] and condensed phase water was removed by heating the crystals to  $\sim 10^\circ\text{C}$ . The remaining particles were presented to the PALMS instrument. Several thousand background aerosol particles were normally analyzed before and after experiments with the CFDC for comparison to the subset which nucleated ice.

The categorization of all INSPECT ice nuclei spectra using a regression tree method [42] showed the two most common categories were mineral dust and fly ash ( $\sim 33\%$ ) and metallic particles ( $\sim 25\%$ ) [12]. Approximately, 5% of particles could not be definitively identified and the remainder contained sulfates, organics and potassium, the later most likely of biomass burning origin [24]. This is in good agreement with previous studies using electron microscopy of collected ice-phase precipitation and atmospheric sampling [13]. Two spectra, typical for the two most populous categories, are shown in Fig. 5. Panel A represents a mineral dust or fly ash particle; there are large peaks due to common mineral components, such as silicon, sodium, calcium and iron as well as oxides. Panel B represents a metallic particle, which nucleated ice. In this case, the major peaks of the spectrum are consistent with those found in panel A but include metals, such as magnesium, aluminum and the unique isotopic signature of zinc at masses 64, 66 and 68.

Murphy et al. [38] described a method to infer the density of a particle given the optical diameter, specified by the scattered signal from the PALMS detection beam, the aerodynamic diameter and the chemical composition. The scattered light versus vacuum aerodynamic diameter is plotted for organic particles, that is those for which the spectra almost exclusively contained organic fragments, analyzed in both positive and negative ion mode, in Fig. 6. This distribution depends on the data in Fig. 4 to the extent that  $d_{va}$  is directly derived from the transit time. The shape factors for such particles is not directly determined

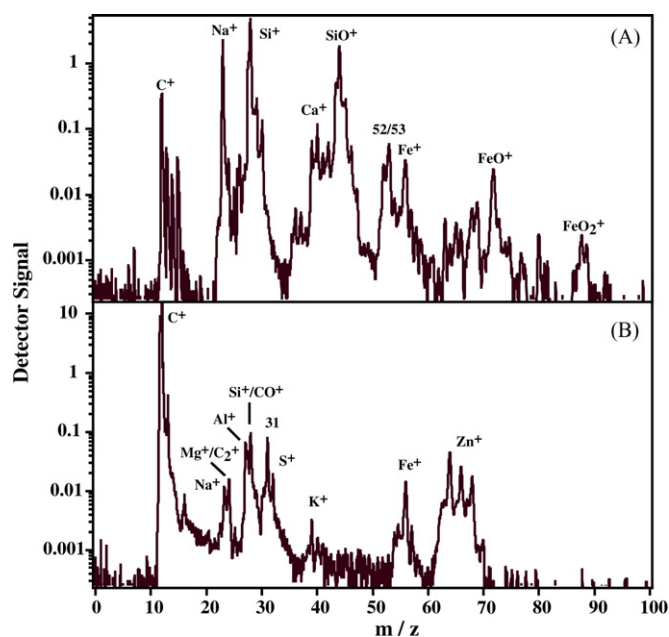


Fig. 5. Mass spectra typical of particles, which were categorized in the two most populous classes of heterogeneous ice nuclei at Storm Peak Laboratory. Panel A: Mineral dust or fly ash (33%) and panel B: metallic (25%). The detector signal in this case is plotted on a log scale.

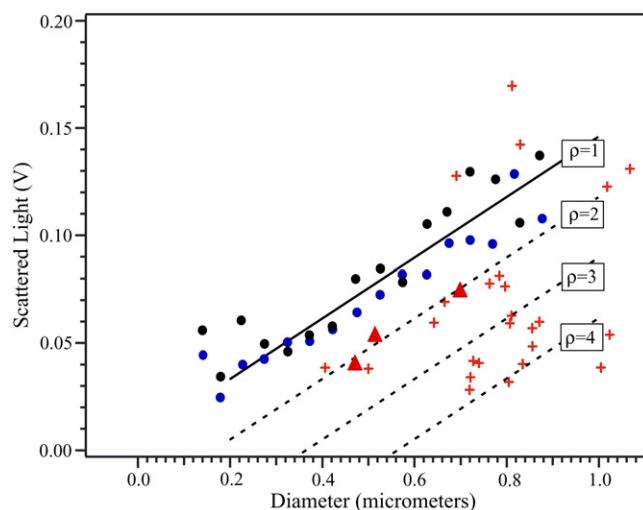


Fig. 6. The height of the scattering signal from the detection beam vs. particle vacuum aerodynamic diameter according to the method of Murphy et al. [38]. Predominantly organic particles acquired from the background atmosphere at Storm Peak Laboratory in positive (black circles,  $\sim 2000$  spectra) and negative polarity (blue circles,  $\sim 1500$  spectra) are grouped in  $0.05\ \mu\text{m}$  diameter bins. The solid line represents a fit through these data and assumes a density of  $\sim 1\ \text{gm cm}^{-3}$ . Dashed lines represent the aerodynamic diameter of higher density spherical particles with the same geometric diameter. Points for experiments with Arizona test dust, conducted at SPL, are plotted as red triangles. Ice nuclei are plotted as red crosses. Data are restricted to those particles, which produced a mass spectrum, returned a timing signal and were analyzed during experiments when the background aerosol was also sampled. Note that it is assumed particles are spherical and have similar refractive indices. Most IN exhibit a density between 2 and  $4\ \text{gm cm}^{-3}$ .

but is assumed spherical and the density to be  $\sim 1 \text{ gm cm}^{-3}$  [38]. In this special case, the physical and aerodynamic diameter are equivalent and a linear fit through these data is plotted as a solid line. According to Eq. (1), dashed lines represent the shift in aerodynamic diameter expected for spherical particles with the same geometric diameter and refractive index but a higher density. Data acquired during experiments with Arizona test dust are plotted as red triangles. The density inferred for these particles is  $\sim 2 \text{ gm cm}^{-3}$  although the MSDS indicates a somewhat higher bulk density ( $\sim 2.5 \text{ gm cm}^{-3}$ ). This may be due to non-spherical or refractive index differences. Ice nuclei are plotted as red crosses and the majority return a density in the range from 2 to  $4 \text{ gm cm}^{-3}$ . The bulk density of most minerals is in the range from 2 to 3 while that of ores and metals is typically 3–4 and sometimes greater than  $5 \text{ gm cm}^{-3}$ . It is interesting to note that those ice nuclei with large light scattering (i.e., those that lie above the  $\rho = 1$  line) also have spectra with mineral dust and metallic components. This probably indicates particles with high density but also highly non-spherical shape as is the case for fractal soot particles.

For comparative purposes electron microscope grids were collected during the INSPECT studies. A NOAA-designed conventional impactor with a total of 24 possible EM grid sites was used. The impactor was operated at a flow rate of  $0.51 \text{ min}^{-1}$  providing a 50% lower cutpoint at  $100 \text{ nm}$  diameter. Grid analyses were performed by the RJ Lee Group, Inc. (Monroeville, PA) using a JEOL Model XX equipped with an energy dispersive spectrometer. Fig. 7 panel A is a histogram of the geometric maximum dimension of 133 IN collected and analyzed during INSPECT-II. The labels on the histogram represent the lower limit of that bin (e.g., bin 0.7 contains particles from this size up to, but not including,  $0.8 \mu\text{m}$  diameter). Although the maximum dimension is plotted it is worth noting that the peak of the minimum dimension also occurs within the  $0.2 \mu\text{m}$  bin and the histogram has the same form. This supports the assumption of roughly spherical IN for this comparison.

The aerodynamic size distribution of ice nuclei observed at Storm Peak is shown in panel B. It can be seen that the peak of this distribution occurs in the  $0.7 \mu\text{m}$  diameter bin. No particles with a diameter less than  $0.4 \mu\text{m}$  were observed to nucleate ice. It is worth noting that this is a vacuum aerodynamic diameter and given the inferred density for IN the smallest detected particles are close in geometric size to the lower detection threshold of the instrument. The upper distribution bound at  $1.1 \mu\text{m}$  diameter can be attributed to the use of a cyclone impactor, also used upstream of the EM grid impactor, to remove material with a 50% cutpoint at  $1.0 \mu\text{m}$  diameter in order to avoid confusion with large ice crystals within the CFDC [25].

A solid line representing the peak of the IN population found for the EM study and with a density of  $1 \text{ gm cm}^{-3}$  and a diameter of  $0.2 \mu\text{m}$  is also plotted in panel B. Subsequent dashed lines represent the aerodynamic diameter of particles with this geometric diameter but with densities from 2 to 4. The peak of the mode observed at Storm Peak is consistent with a density between 3 and 4, which is qualitatively in agreement with the estimate made using Fig. 6.

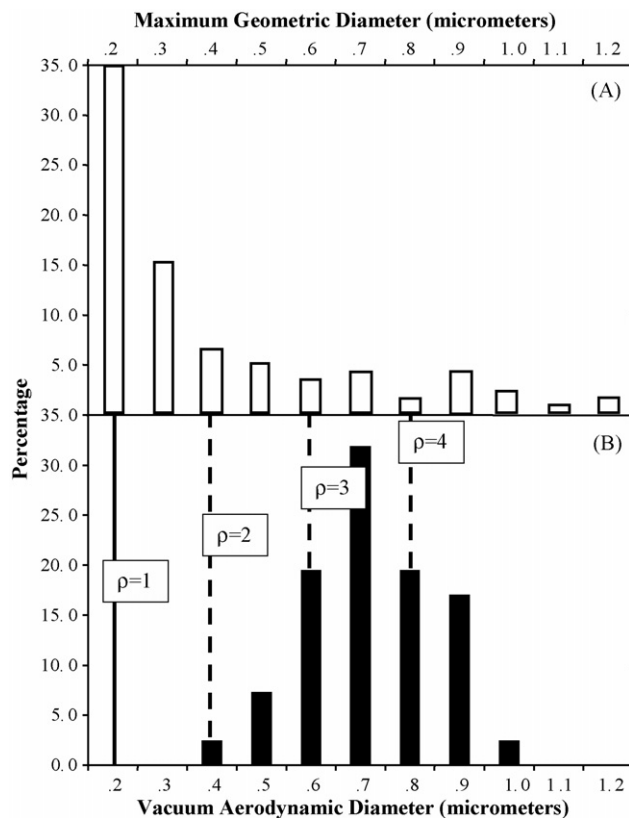


Fig. 7. Histograms of the ice nucleus distribution as a function of diameter at Storm Peak Laboratory. The open bars in panel A represent the geometric maximum dimension distribution for ice nuclei collected during INSPECT-II (see text for details). The solid bars in panel B represents the vacuum aerodynamic diameter determined using the PALMS instrument. The median geometric diameter, assuming spherical particles and a density of unity, from the electron microscope study is plotted with a solid line in the  $0.2 \mu\text{m}$  bin. Dashed lines represent the aerodynamic diameter of higher density spherical particles with the same geometric diameter. Note that the data from Fig. 6 suggest that a density between 2 and 4 is a good estimate for IN.

There are several other comprehensive studies of ice forming aerosols using electron microscopy (e.g., [15] and references therein). There are two reasons that the most applicable for comparison to these data is that of Chen et al. [13]. First, that study took place from a NASA DC-8 platform over the central United States, which was also the location of the INSPECT field campaigns. Second, ice crystals were formed within the same CFDC instrument used for the INSPECT studies. In all other studies, ice crystals were collected from atmospheric ice clouds or precipitation, which means the exact formation temperature and saturation and scavenging events remain unknown. Chen et al. [13] used EM to size and energy dispersive X-ray analysis to determine composition of ice nuclei. The lower detectable size limit was  $0.05 \mu\text{m}$  geometric diameter whereas the lower compositional limit was  $0.1 \mu\text{m}$ . The upper limit in both cases was set by an impaction stage upstream of the CFDC with a  $2 \mu\text{m}$  cutpoint. Chen et al. [13] reported a mode size for IN at  $\sim 0.2 \mu\text{m}$ , equivalent to that found during INSPECT, and noted that there were greatly diminished loadings of particles smaller than  $0.1 \mu\text{m}$ . The chemical character of the IN was enriched in crustal and metallic particles with respect to the background aerosol.

#### 4. Conclusions

Here we describe the design and implementation of several modifications to the PALMS instrument, a conventional laser desorption/ionization aerosol mass spectrometer, in order to study low number density species. This technique has been successfully used to determine the chemical composition of those particles which nucleated ice under controlled temperature and relative humidity conditions at a remote mountain-top field location and from a high altitude research aircraft. In the most extreme situations, as few as one aerosol particle per liter nucleated ice, were inertially separated from those particles which did not nucleate ice, and were subsequently analyzed using aerosol mass spectrometry. In such cases, approximately two particles were sized and produced mass spectra per hour.

The ability to ascertain the chemical composition of low number density species is important to several contemporary issues in atmospheric science beyond the formation of the ice phase. One example is the determination of the dependence of hygroscopic growth on particle composition. This topic has been addressed by coupling a Humidified Tandem Differential Mobility Analyzer (HTDMA) to an aerosol mass spectrometer to first size select and then expose those particles to controlled relative humidity conditions [43]. Particles were again size selected using the second of the tandem DMAs and chemical composition determined as a function of growth factor. Because of the multiple size selection steps and the elemental charge restrictions inherent to a DMA, the output of aerosols in such an experiment was several of orders of magnitude less than that found in the environment [44].

#### Acknowledgements

This work was supported by NSF (grants ATM-0124927 and ATM-0334228; any opinions, findings and conclusions expressed in this material are those of the authors and do not necessarily reflect the views of NSF), PECASE and NOAA funding. We wish to thank Karl Froyd, Stephane Gallavardin, Paula Hudson, Jose Jimenez, Richard McLaughlin and Mike Schein for their invaluable assistance on this project.

#### References

- [1] M.P. Sinha, S.K. Friedlander, *Anal. Chem.* 57 (1985) 1880.
- [2] P.J. McKeown, M.V. Johnston, D.M. Murphy, *Anal. Chem.* 63 (1991) 2069.
- [3] K.P. Hinz, R. Kaufmann, B. Spengler, *Anal. Chem.* 66 (1984) 2071.
- [4] B.A. Mansoori, M.V. Johnston, A.S. Wexler, *Anal. Chem.* 66 (1994) 3681.
- [5] D.S. Thomson, D.M. Murphy, *Chem. Tech.* 24 (1994) 30.
- [6] E.E. Gard, M.J. Kleeman, D.S. Gross, L.S. Hughes, J.O. Allen, B.D. Morrical, D.P. Fergenson, T. Dienes, M.E. Galli, R.J. Johnson, G.R. Cass, K.A. Prather, *Science* 279 (1998) 1184.
- [7] D.M. Murphy, J.R. Anderson, P.K. Quinn, L.M. McInnes, F.J. Brechtel, S.M. Kreidenweis, A.M. Middlebrook, M. Pósfai, D.S. Thomson, P.R. Buseck, *Nature* 392 (1998) 62.
- [8] D.M. Murphy, D.S. Thomson, M.J. Mahoney, *Science* 282 (1998) 1664.
- [9] J.H. Seinfeld, S.N. Pandis, *Atmospheric Chemistry and Physics: From Air Pollution to Climate Change*, Wiley-Interscience, New York, 1998, p. 430.
- [10] *Scientific Assessment of Ozone Depletion: 1998*, World Meteorological Organization Report No. 44, Geneva, 1999, p. 3.16.
- [11] D. Lynch, K. Sassen, D. Starr, G.L. Stephens (Eds.), *Cirrus*, Oxford University Press, New York, 2002, p. 3.
- [12] P.J. DeMott, D.J. Cziczko, A.J. Prenni, D.M. Murphy, S.M. Kreidenweis, D.S. Thomson, R. Borys, D.C. Rogers, *Proc. Natl. Acad. Sci.* 100 (2003) 14655.
- [13] Y. Chen, S.M. Kreidenweis, L.M. McInnes, D.C. Rogers, P.J. DeMott, *Geophys. Res. Lett.* 25 (1998) 1391.
- [14] H.R. Pruppacher, J.D. Klett, *Microphysics of Clouds and Precipitation*, second ed., Kluwer Academic, Netherlands, 1998, p. 317.
- [15] C.H. Twohy, M.R. Poellot, *Atmos. Chem. Phys. Discuss.* 5 (2005) 3723.
- [16] P.A. Baron, K. Willeke (Eds.), *Aerosol Measurement*, second ed., Wiley-Interscience, New York, 2001, p. 295.
- [17] M.V. Johnson, *J. Mass Spectrom.* 35 (2000) 585.
- [18] D.S. Thomson, A.M. Middlebrook, D.M. Murphy, *Aerosol Sci. Technol.* 26 (1997) 544.
- [19] D.S. Thomson, M.E. Schein, D.M. Murphy, *Aerosol Sci. Technol.* 33 (2000) 153.
- [20] A.M. Middlebrook, D.S. Thomson, D.M. Murphy, *Aerosol Sci. Technol.* 27 (1997) 293.
- [21] D.S. Thomson, D.M. Murphy, *Appl. Opt.* 32 (1993) 6818.
- [22] D.M. Murphy, D.S. Thomson, *J. Geophys. Res.* 102 (1997) 6353.
- [23] D.M. Murphy, D.S. Thomson, *J. Geophys. Res.* 102 (1997) 6341.
- [24] P.K. Hudson, D.M. Murphy, D.J. Cziczko, D.S. Thomson, J.A. de Gouw, C. Warneke, J. Holloway, H.J. Jost, G. Hubler, *J. Geophys. Res.* 109 (2004) D23S27, doi:10.1029/2003JD004398.
- [25] D.J. Cziczko, P.J. DeMott, C. Brock, P.K. Hudson, B. Jesse, S.M. Kreidenweis, A.J. Prenni, J. Schreiner, D.S. Thomson, D.M. Murphy, *Aerosol Sci. Technol.* 37 (2003) 460.
- [26] D.J. Cziczko, D.M. Murphy, P.K. Hudson, D.S. Thomson, *J. Geophys. Res.* 109 (2004) D04201, doi:10.1029/2003JD004032.
- [27] J.E. Boulter, D.J. Cziczko, A.M. Middlebrook, D.S. Thomson, D.M. Murphy, *Aerosol Sci. Technol.*, in press.
- [28] J. Schreiner, C. Voigt, P. Zink, A. Kohlmann, D. Knopf, C. Weisser, P. Budz, K. Mauersberger, *Ref. Sci. Inst.* 73 (2002) 446.
- [29] P. Liu, P.J. Ziemann, D.B. Kittelson, P.H. McMurry, *Aerosol Sci. Technol.* 22 (1995) 314.
- [30] J.T. Jayne, D.C. Leard, X. Zhang, P. Davidovits, K.A. Smith, C.E. Kolb, D.R. Worsnop, *Aerosol Sci. Technol.* 33 (2000) 49.
- [31] A. Zelenyuk, D. Imre, *Aerosol Sci. Technol.* 39 (2005) 1.
- [32] Y. Su, M.F. Sipin, H. Furutani, K.A. Prather, *Anal. Chem.* 76 (2004) 712.
- [33] P.F. DeCarlo, J.G. Slowik, D.R. Worsnop, P. Davidovits, J.L. Jimenez, *Aerosol Sci. Technol.* 38 (2004) 1185.
- [34] C.M. Archuleta, P.J. DeMott, S.M. Kreidenweis, *Atmos. Chem. Phys. Discuss.* 5 (2005) 3391.
- [35] J.L. Jimenez, J.T. Jayne, Q. Shi, C.E. Kolb, D.R. Worsnop, I. Yourshaw, J.H. Seinfeld, R.C. Flagan, X. Zhang, K.A. Smith, J. Morris, P. Davidovits, *J. Geophys. Res.* 108 (2003) 8425, doi:10.1029/2001JD001213.
- [36] J.A. Huffman, J.T. Jayne, F. Drewnick, A.C. Aiken, T. Onasch, D.R. Worsnop, J.L. Jimenez, *J. Aerosol Sci.* 39 (2005) 1143.
- [37] J. Herberlein, *Surf. Coat. Technol.* 142 (2001) 265.
- [38] D.M. Murphy, D.J. Cziczko, P.K. Hudson, M.E. Schein, D.S. Thomson, *J. Aerosol Sci.* 35 (2004) 135.
- [39] D.S. Thomson, R. Winkler, *Sci. Comp. Inst.* (1999) 54.
- [40] J. Conway, S. Watts, *A Software Engineering Approach to LabVIEW*, Prentice Hall, New Jersey, 2004, pp. 34–58.
- [41] D.C. Rogers, *J. Atmos. Oceanic Technol.* 11 (1994) 1042.
- [42] D.M. Murphy, A.M. Middlebrook, M. Warshawsky, *Aerosol Sci. Technol.* 37 (2003) 382.
- [43] G. Buzorius, A. Zelenyuk, F.J. Brechtel, D. Imre, *Geophys. Res. Lett.* 29 (2002) 1974, doi:10.1029/2001GL014221.
- [44] F.J. Brechtel, S.M. Kreidenweis, *J. Atmos. Sci.* 57 (2000) 1854.